Cracking the Code of Pre-Earthquake Low Frequency EM Emissions

Friedemann T. Freund[1,2], Akihiro Takeuchi[2,3], Bobby W.S. Lau[2]

[1] NASA Goddard Space Flight Center, Planetary Geodynamics Laboratory, Code 698 Greenbelt, MD 20771, USA, ffreund@core2.gsfc.nasa.gov

[2] San Jose State University, Department of Physics, San Jose, CA 95192-0106, USA
[3] Niigata University, Department of Chemistry, Niigata 950-2181, Japan

Abstract

The basis of many non-seismic pre-earthquake signals, in particular low frequency electromagnetic (EM) emissions, are transient electric currents that flow in the Earth's crust. We show that, when we apply stresses to one end of a block of igneous rocks, two currents flow out of the stressed rock volume. One current is carried by electrons and it flows out through a Cu electrode directly attached to the stressed rock volume. The other current is carried by p-holes, i.e. defect electrons on the oxygen anion sublattice, and it flows out through at least 1 m of unstressed rock. The two currents are coupled via their respective electric fields and fluctuate. Applying the insight gained from these laboratory experiments to the field, where large volume of rocks are subjected to ever increasing stress, leads us to suggest transient, fluctuating currents of considerable magnitude that would build up in the Earth's crust prior to major earthquakes.

Introduction

A recent Letter in Nature (Gerstenberger et al., 2005) begins with the words: "Despite a lack of reliable deterministic earthquake precursors, seismologists have significant predictive information about earthquake activity from an increasingly accurate understanding of the clustering properties of earthquakes." This statement alludes to the fact that, when earthquakes happen, they are chaotic events. Their chaotic character is exacerbated by the heterogeneity of the Earth's crust, particularly along seismically active plate margins, which are crisscrossed by faults and pot-marked by deeply buried asperities. When and where a given fault segment will fail depends on processes that take place under kilometers of rock. Unless there is a history of prior seismic activity that leaves a trail of signals, it is unknowable where faults go at depth and when asperities might fail. Therefore, the tools of seismology can cast time and approximate location of the next earthquakes only in terms of statistical probability.

However, there is a non-seismological approach, which can add to our knowledge base. In this approach we attempt to understand the electromagnetic signals, if any, that the Earth reportedly sends out before major earthquakes.

The literature is replete with reports of pre-earthquake phenomena. Some of these phenomena can be explained mechanistically by assuming that, when large volumes of rock are squeezed deep underground, they deform plastically and develop microfracture leading to the well-publicized dilatancy theory (Brace, 1975; Brace et al., 1966; Hazzard et al., 2000) that can account for the bulging of the Earth's surface, for changes in well-water levels (Chadha et al., 2003; Igarashi et al., 1993; Igarashi and Wakita, 1991), in the outpour of hot springs (Biagi et al., 2001; Goebel et al., 1984), and in the composition of the gases dissolved in spring waters (Hauksson, 1981; Igarashi et al., 1993; Plastino et al., 2002; Rao et al., 1994; Sano et al., 1998).

Other pre-earthquake phenomena cannot be explained mechanistically such as low-frequency electromagnetic (EM) emissions (Fujinawa et al., 2001; Fujinawa and Takahashi, 1990; Gershenzon and Bambakidis, 2001; Gokhberg et al., 1982; Molchanov and Hayakawa, 1998; Nitsan, 1977; Vershinin et al., 1999; Yoshida et al., 1994; Yoshino and Tomizawa, 1989), local magnetic field anomalies (Fujinawa and Takahashi, 1990; Gershenzon and Bambakidis, 2001; Ivanov et al., 1976; Kopytenko et al., 1993; Ma et al., 2003; Yen et al., 2004; Zlotnicki and Cornet, 1986), increases in radio-frequency noise (Bianchi and al., 1984; Hayakawa, 1989; Martelli and Smith, 1989; Pulinets et al., 1994), and earthquake lights (Derr, 1973; King, 1983; St-Laurent, 2000; Tsukuda, 1997; Yasui, 1973). This group of pre-earthquake signals requires electric currents in the ground. Sometimes the strength of the recorded signals, in particular low frequency EM emissions, require strong currents. All past attempts to identify a physical process that could generate strong currents deep in the ground have not produced convincing results.

Here we describe a simple experiment that subjects igneous rocks (granite, anorthosite, gabbro) to stress. By judiciously connecting electrodes to the rocks we show that electric currents are generated, which flow out of the stressed rock volume without externally applied voltage. These self-generated currents may hold the key to understand how powerful electric currents can be generated deep in the Earth prior to major earthquakes and what kind of signals they send out.

Experimental

Figure 1a shows a long granite slab, 1.2 m long with a rectangular 10 x 15 cm^2 cross section, *in situ* in a press, electrically insulated from the two pistons by means of two 0.8 mm thick hard polyethylene sheets with a resistance of $>10^{14}$ Ω. The load was applied uniaxially to one end of the slab between two pistons, 11.25 cm diameter, stressing a volume of ~1500 cm^3. The rock was fitted with two Cu tape electrodes with graphite-based, conductive adhesive, each connected to an ampere meter. One electrode surrounded the back end of the rock so that the volume to be stressed was in electrical conduct with the Cu electrode and, hence, with ground. The other electrode of the same size wrapped around the front end of the rock. In addition we had placed a non-contact capacitive sensor on the top of the rock, made with the same Cu tape and 0.8 mm thick polyethylene insulator. **Figure 1b** shows the corresponding electric circuit that is designed to allow stress-activated currents to flow out of the stress rock volume.

The back end of the slab was loaded uniaxially at a constant rate of about 6 MPa/min to a maximum stress level of 67 MPa, equal to about 1/3 the failure strength of the granite. The load was applied repeatedly, a total of 6 times, with 30 min between loading/unloading cycles.

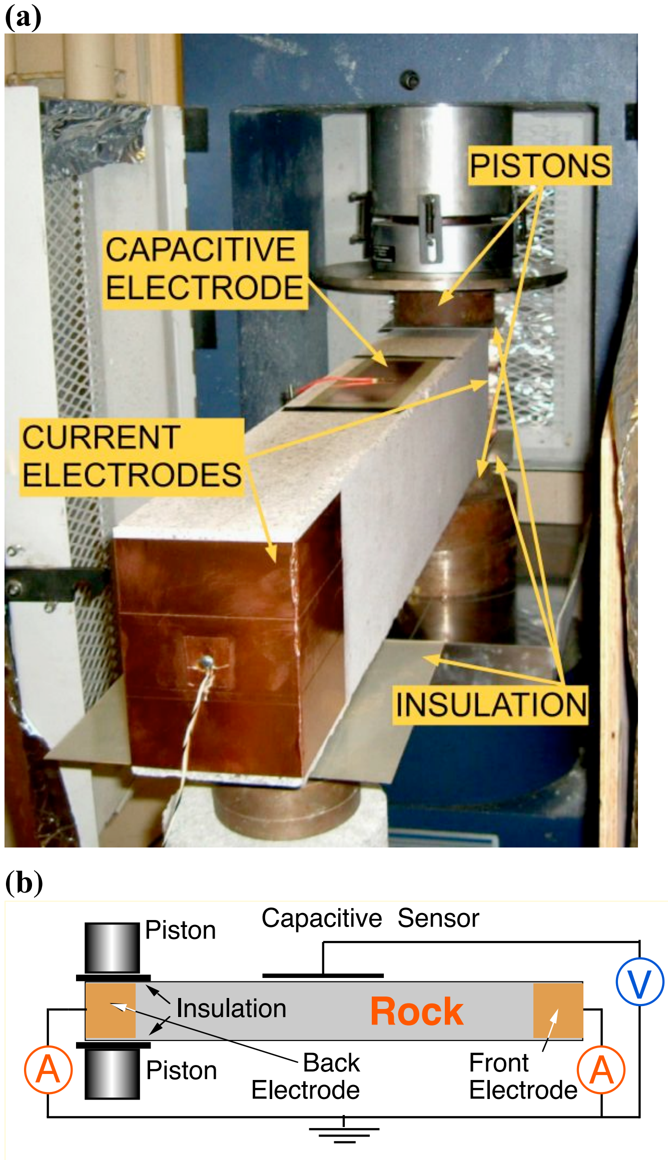

Figure 1a: *Granite slab placed in the press, ready for the uniaxial compression tests. The granite slab (1.2 m long, 10 x 15 cm^2 cross section) is fitted with two Cu electrodes (each 30 x 15 cm^2), one at the back end and one at the front end, plus a non-contact capacitative sensor for measuring the surface potential. The rock is insulated from the pistons and the press by 0.8 mm thick polyethylene sheets (>10^{14} Ωcm).*

(b): *Block diagram of the electric circuit for allowing the self-generated currents to flow out of the stressed rock volume.*

To measure the outflow currents we used two Keithley ampere meters, model 486 and 487. To measure the surface potential we used a Keithley electrometer, model 617. The data were acquired with National Instrument LabVIEW 7.0.

The experiment was carried out with dry, light-gray, medium-grained "Sierra White" granite from Raymond, CA, containing ca. 30 modal% quartz, 30% microcline, 20% plagioclase, and 10% amphibole. Similar experiments not described in detail here were carried out with centrally loaded 30 x 30 x 0.95 cm^3 rock tiles of the same granite and with other igneous quartz-free rocks such as a coarse-grained anorthosite from Larvik, Norway, and a black, fine-grained gabbro from Shanxi, China. In addition we used a white Carrara marble and plate glass for reference.

III Results and Discussion

III.1 Two Currents

When we stress one end of the granite block fitted with the two Cu electrodes, two currents begin instantly to flow out of the stressed rock volume. The currents are of same magnitude, but of opposite sign. They flow out in opposite directions without any externally applied voltage. They increase with increasing stress.

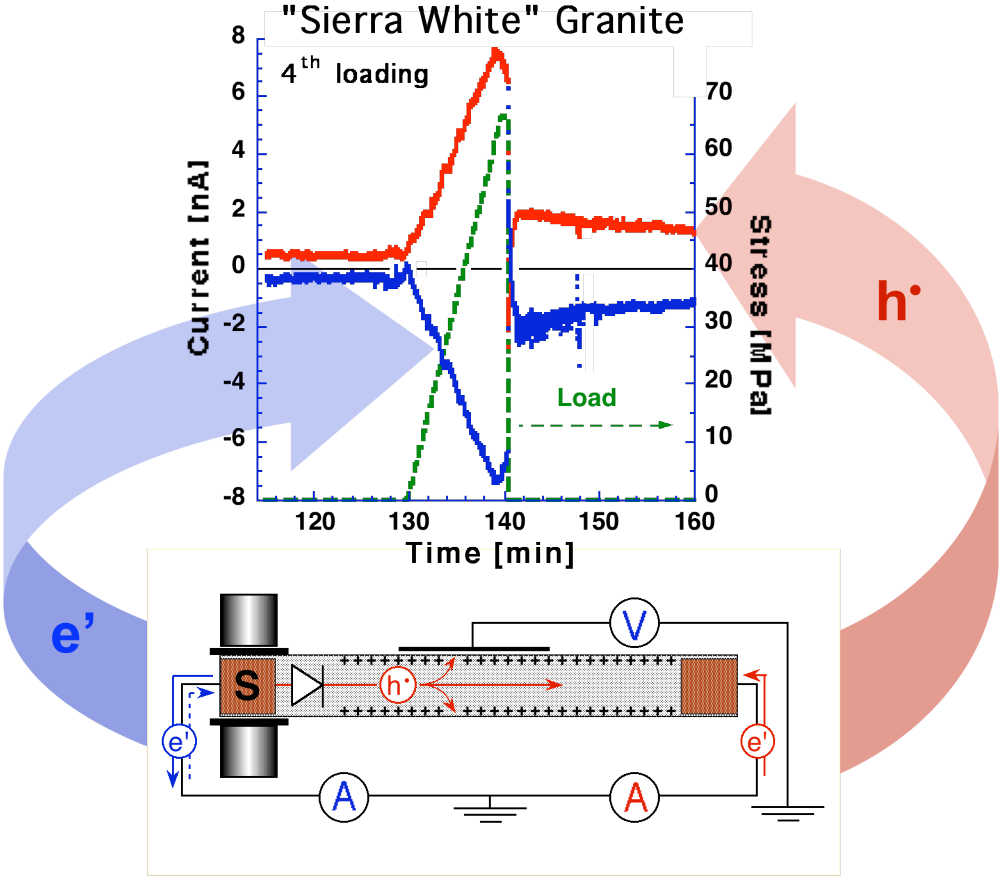

Figure 2: *Two currents flowing out of the stressed rock volume, the "source" S, and a schematic representation of the current flow through the external circuit and inside the rock passing through the interface between stressed/unstressed rock which acts as a barrier for electrons.*

We repeated the loading/unloading cycle six times and always observe the same two currents. **Figure 2** summarizes the results of the 4th loading/unloading cycle**.** The current trace in blue and marked by the blue arrow is carried by electrons. It flows from the stressed rock volume, the "source" (S), directly into the Cu electrode that is attached to the back end of the granite slab and thence to ground. The other current trace in red and marked by the red arrow is carried by defect electrons, i.e. by holes. The hole current flows from the source through the full length of the granite slab, through ~1 m of unstressed rock, to the front Cu electrode and thence to ground. The source volume contains ~1500 cm^3 of rock. Stressing this volume to 67 MPa, about 1/3 the failure strength of the granite, leads to peak currents of ~7 nA. Other igneous rocks such as the anorthosite and gabbro produced larger currents, by a factor of 10-50.

On releasing the load both currents drop precipitously but do not return to near-zero. Instead they drop to about ¼ their peak value and then decay slowly. The 30 min at zero load between each loading/unloading cycle are not long enough to allow the currents to decay to zero. Therefore the starting levels for the outflow currents increase with each cycle, leading to ever higher peak currents. Eventually, the peak currents reach a maximum. In similar experiments where we loaded and unloaded granite and other rocks at constant rates, the outflow currents after unloading returned to near-zero and the peak currents reach always the same maximum values even after more than 20 cycles.

The outflow of two currents implies that mechanical stress activates two types of electronic charge carriers, electrons and holes, presumably in equal numbers. The holes are able to flow through ~1 m of unstressed granite, while the electrons are blocked from entering the unstressed portion of the rock. Instead they flow out via the Cu electrode that is directly attached to the stressed rock volume.

This dual outflow in opposite directions implies an energy barrier between the stressed and unstressed rock, which allows only holes to pass through. This energy barriers probably plays an important role in setting up and sustaining the observed dual current flow pattern.

III.2 Electrons and Positive Holes

Before a current can flow, charge carriers have to be created or activated in the stressed rock volume. Since the charge carriers did not exist before, we conclude that the rock contains inactive precursors that can be “awakened” by the application of stress.

Prior work (Freund, 2003) has already brought us a better understanding of the hole-type charge carriers that lie dormant in igneous rocks. These holes are defect electrons in the O^{2-} sublattice of silicate minerals, known as “positive holes” or p-holes for short, and symbolized by $h^{\bullet}$.

A defect electron in the O^{2-} sublattice can be described as O^{-} in a matrix of O^{2-}, i.e., as an electronic state where the valence of oxygen has changed from 2– to 1–. In their dormant state p-holes exist as pairs, in the form of peroxy bonds, O^{-}–O^{-}, or peroxy links, $O_3X/^{OO}\backslash XO_3$, $X=Si^{4+}$, Al^{3+} etc., which we call “positive hole pairs” or PHP. We know that these PHPs can be activated by stress and that they release mobile p-hole charge carriers (Freund, 2002).

However, the experiment described here demonstrates co-activation of holes and electrons. To understand this process we need to take a closer look at the PHPs and their electronic structure.

As indicated by its position in the Periodic Table of the Elements, oxygen has the electronic configuration $1s^2|2s^2p^4$, where 6 electrons to the right of the vertical bar form the valence shell. When oxygen is in its most common 2– oxidation state, its electronic configuration becomes $1s^2|2s^2p^6$, meaning that it now has the closed-shell 8 valence electron configuration of the noble gas neon. When oxygen is in its 1– oxidation state, its electronic configuration is $1s^2|2s^2p^5$ with an odd number of valence electrons. Such a 7-electron configuration is unstable. It can stabilize by pairing with another O^{-} to form a peroxy bond, O^{-}–O^{-}, with 14 valence electrons.

We use Molecular Orbitals (MO) to examine more closely the electronic structure of the peroxy bond. **Figure 3a** depicts on the left side the MO energy levels of a peroxy entity, O_2^{2-}, flanked by the energy levels of two O^{-}, each with $1s^2|2s^2p^5$ electrons (Marfunin, 1979). The AOs of the two O^{-}combine to form bonding, non-bonding and antibonding levels (superscript ^{b}, ^{nb}, and *, respectively). Bonds that derive primarily from the 2s and $2p_z$ AOs (z being the bond direction between the two O^-) are called σ. In bonding σ orbitals, σ^b, the electron density is between the two O^-. In antibonding σ orbitals, σ^*, the electron density is highest outside the O^-–O^- bond. The MOs called π represent double bonds, which derive primarily from the $2p_x$ and $2p_y$ AOs. The π MOs form a torus of electron density around the –O–O– axis. One set is weakly bonding, π^b, the other set is non-bonding, π^{nb}.

A hallmark of the peroxy bond is that its highest MO, the strongly antibonding σ^*, is empty. Hence the peroxy bond lacks the strongly repulsive electron density of an occupied σ^* level. As a result the O^-–O^- bond is highly covalent and the O^-–O^- bond distance much shorter than the usual distance between adjacent O^{2-} in oxide and silicate minerals, ~1.5 Å versus 2.8-3.0 Å.

Next we ask: what happens when the peroxy bond breaks? At least two reaction channels are available. One is followed when bulk peroxides such as BaO_2 are heated above 600°C and decompose, $BaO_2 \rightarrow BaO + ½ O_2$. Its basic step involves a regroupment of the electrons among the two O^- in such a way as to split (disproportionate) their valence states, $O^- + O^- \rightarrow O^{2-} + O$. Such disproportionation reaction can take place only on the surface of solid grains. It leads as its primary step to the emission of O atoms (Martens et al., 1976).

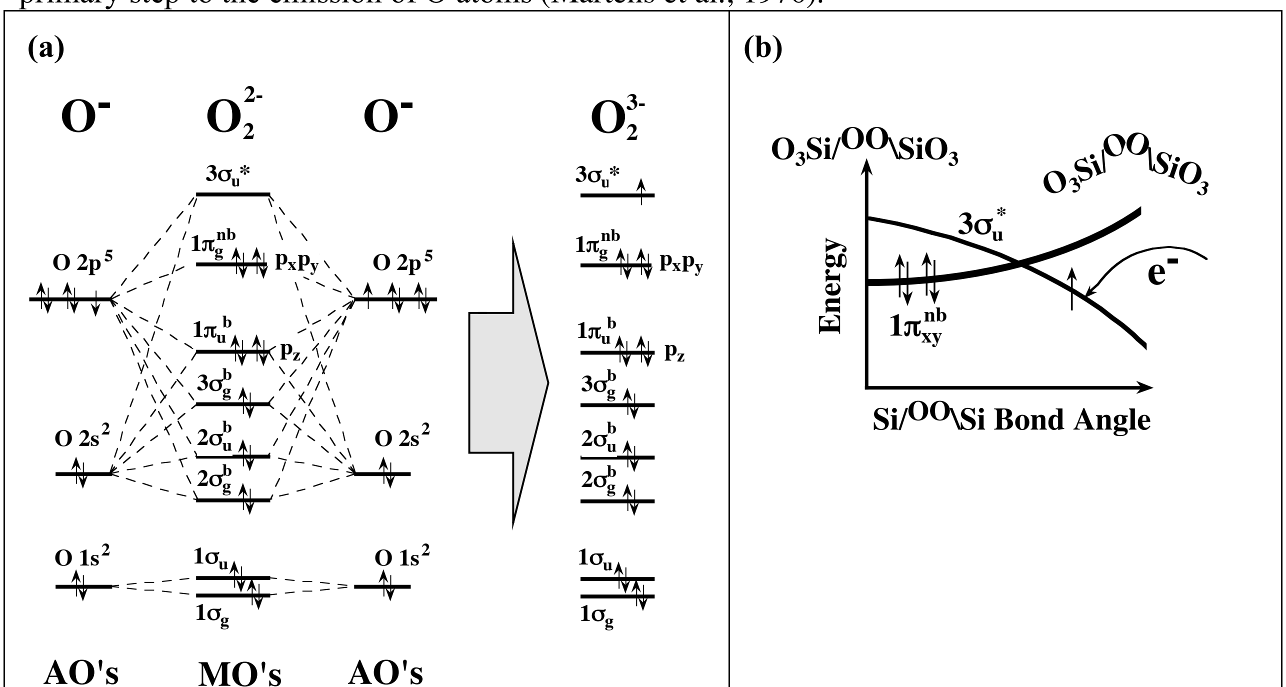

Figure 3a: *Schematic representation of the energy levels of the bonding, non-bonding and antibonding molecular orbitals in the peroxy anion,* O_2^{2-} *and* O_2^{3-} *using Molecular Orbital concepts (see text).*

Figure 3b: *Schematic representation of how the high-lying antibonding orbital decreases in energy and the highest occupied non-bonding orbital increases when the peroxy bond is bent.*

The other channel of more direct relevance here is open to peroxy entities imbedded in the O^{2-} matrix of an oxide or silicate crystal. When dislocations move through a mineral grain during plastic deformation, they intersect peroxy links and briefly "wiggle" the $O_3X/^{OO}\backslash XO_3$ entities, i.e. change their $X/^{OO}\backslash X$ bond angle. Any change in the $X/^{OO}\backslash X$ angle leads to a decrease in the energy of the high-lying antibonding σ^* orbital and to an increase in the energy of lower-lying bonding and non-bonding π^{nb} orbitals (Marfunin, 1979) as indicated schematically in **Figure 3b**.

Every matrix-imbedded peroxy entity is surrounded by next-nearest O^{2-}, each with fully occupied high-lying levels that are of repulsive, antibonding $(sp)^*$ character. When the energy of the empty σ^* level of the peroxy entity drops below the energy of the highest occupied $(sp)^*$ levels of any of its next-nearest O^{2-} neighbor, an electron from the O^{2-} can transition into the σ^* level of the strained peroxy bond. Such electron transfer onto the peroxy entity creates a hole on the neighboring O^{2-}, i.e. turns this O^{2-} into an O^-. Hence, one electron hopping into the peroxy bond is equivalent to one hole hopping out.

Such electron transfer may represent the basic step of how an imbedded peroxy entity can inject a hole into the O^{2-} sublattice and thereby releases a p-hole charge carrier into the valence band.

The spreading of the $h^\bullet$ state away from its parent peroxy entity is probably facilitated by the fact that the wave function associated with the $h^\bullet$ is highly delocalized (Freund et al., 1994). By spreading over many O^{2-} sites, the $h^\bullet$ dilutes its charge density and thereby minimizes the electrostatic interaction with the parent peroxy defect, left behind with an extra electron, i.e. as a negatively charged point defect. This extra electron sits on the antibonding σ^* orbital as reported by Symon (Symons, 2001). On the right side of the arrow in **Figure 3a** we have sketched the MO diagram fro this configuration with a single, unpaired electron on the high-lying σ^* level, though its energy is certainly different from that with an empty σ^* orbital.

When we apply the same rationale to the peroxy link between adjacent XO_4, the energy levels split due to the lower symmetry but the principle remains the same. We symbolize the extra electron by superscript ‘ next to the peroxy link, $O_3X/^{[OO]'}\backslash XO_3$ and write:

$$O_3X/^{OO}\backslash XO_3 + O^{2-} \rightarrow O_3X/^{[OO]'}\backslash XO_3 + O^- \qquad [1]$$

No calculations seem to have been performed to date to study how the $X/^{[OO]'}\backslash X$ bond angle changes after adding electron. It is possible, even likely, that the $X/^{[OO]'}\backslash X$ bond remains in a permanently bent form, thereby providing some degree of stability to the extra electron and preventing a rapid recombination with the hole that it has just released.

At the same time we have reason to expect that the lone electrons on the σ^* level are loosely bound and therefore represents the mobile electrons that flow out of the stressed rock volume via the Cu electrode attached to the back end on the granite block as shown in **Figure 1**. If this is correct, **Figure 3a/b** and eq. [1] sketch the complete reaction of interest here: (i) the generation of holes that move away from their parent peroxy entities as p-hole charge carriers and (ii) the generation of loosely bound electrons, acquired by the parent peroxy entities in the process of releasing a p-hole.

III.3 What Drives the Current Outflow?

The electric circuit shown at the bottom of **Figure 1** provides the loop that the electrons need to flow from the source volume to ground and thence to the front Cu electrode. At the front Cu electrode the electrons meet the p-holes, which have traveled through ~1 m of granite rock. There must be some mechanism that drives this dual current outflow.

As mentioned above, only p-holes can flow through the unstressed rock, while the electrons have to take the path through the Cu electrode attached to the source volume. The inability of the electrons to flow through the unstressed rock implies a boundary between the stressed and unstressed rock that allows p-holes to pass but blocks electrons.

In the case of the granite slab the two outflow currents increase approximately linearly with the stress as shown by **Figure 2**. During most of the loading the currents fluctuate synchronously, indicating that they are strongly coupled. However, at the beginning there is a difference.

If the fluctuations were synchronous and perfectly balanced, the sum of the two currents should be zero. **Figure 4** shows that the sum of the two currents is zero except for the first 2 min, when electrons are flowing into, not out of, the source volume. This inflowing current peaks early and ends when the load has barely reached 15 MPa. After unloading a reverse current flows out of the source volume in a series of brief bursts. Integration gives 3 x 10^{11} charges flowing in and about the same number, 3.5 x 10^{11}, flowing out.

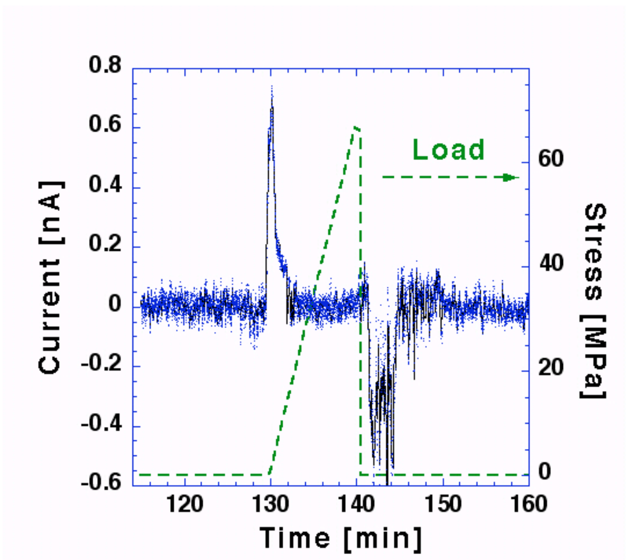

***Figure 4**: Adding the two outflow currents shows that, at the beginning of loading, electrons flow into the source volume. After unloading the same electrons flow out.*

The initial inflow ~3 x 10^{11} electrons into the source volume indicates a driving force. A hint as to what this driving force might be is provided by the positive charges on the surface of the rock. In the experiment described here the surface potential reaches +25 mV. Typical values measured, when currents are drained from the rock, are +10 to +100 mV. Under open circuit conditions the surface potentials measured reach +1.5 to +1.75 V (Takeuchi et al., 2005).

To find a reasonable explanation for the two outflow currents we combine the three observations presented here:

(i) upon loading electrons and holes are co-activated in the source volume,
(ii) p-holes flow out of the stressed rock volume into the adjacent unstressed rock, and
(iii) a positive charge builds up on the surface of the unstressed rock.

Step (ii), the initial outflow of p-holes, occurs in response to the concentration gradient between the source volume and the adjacent unstressed rock. When p-holes expand into a dielectric, they spread to the surface and set up the surface charge (King and Freund, 1984). The number of p-holes spreading out initially should be equal to the number of positive charges needed to set up a surface potential of +25 mV multiplied by the surface area, ~0.5 m^2, of the granite slab under study here. According to Takeuchi and Nakahama (Takeuchi and Nagahama, 2001; Takeuchi and Nagahama, 2002) and Enomoto (Enomoto and Hashimoto, 1990) fractures or stick-slip faulting lead to surface potentials in the range of 10 V, corresponding to charge densities on the order 10^{-5} Coulomb/m^2 or 6 x 10^{13} charges/m^2. Scaling the surface potential from 10 V to 25 mV gives ~10^{11} charges. This is in good agreement with our values, given the uncertainties in measuring surface potentials and in estimating surface charge densities.

The initial outflow of p-holes pulls electrons from ground into the source volume. Thereafter, as the continuous current develops, the electron current reverses, flowing out of the source volume, looping through the outer circuit to the front end of the granite slab where the electrons meet the p-holes. It is possible that this current is driven by the energy gained during recombination of p-holes and electrons at the front Cu electrode. When the load is removed, the electrons, which had initially entered the source, flow back to ground as illustrated by **Figure 4**.

Coupling of the Outflow Currents

The two outflow currents always fluctuate even at constant rates of stress increase. The amplitudes of fluctuations can reach 50% of the mean value. In the case of the 1.2 m long granite slab the fluctuations were less, on the order of 10% or less as shown in **Figure 5**. The fluctuations were synchronous as additionally demonstrated in **Figure 4** by the sum of the outflow currents being zero over much of the 10 min time window except for the first 2 min.

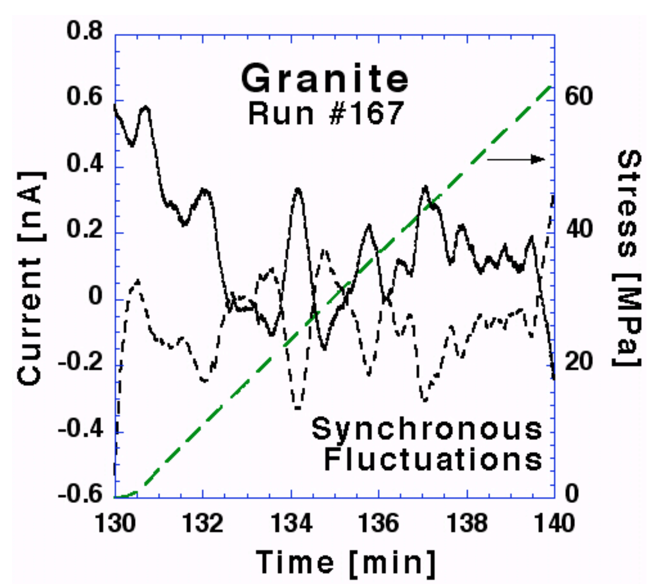

Figure 5: *Synchronous fluctuations of the two outflow currents during most of the loading.*

Synchronous fluctuations imply a strong coupling. The electric fields associated with each of the outflow currents can provide such coupling. The reason is that, when one of the currents varies, the other current reacts by increasing or decreasing in order to minimize the electric field. As a result both currents will fluctuate just as we seem to always see it in our laboratory experiments.

Modeling Pre-Earthquake Situations

We can use our experiment with the 1.2 m long granite slab depicted in **Figure 1a** and the insight gained by this new approach to build a qualitative model of the Earth's crust and of the telluric currents generated as a result of stress–activated electron and p-hole currents. We may scale up the outflow currents from our modest laboratory size (source volume ~1500 cm^3) to geophysically relevant stressed rock volumes. If we do, every km^3 of granite would be able to produce 5 x 10^4 A. Other rocks, in particular gabbro, might produce currents up to 10^6 A/km^3.

We consider a cross section through the crust featuring a 25-30 km thick block that is being pushed horizontally from the left as shown in **Figure 6a**. The stress is assumed to be applied over the entire cross section from the brittle upper crust down to a depth where the rocks, due to increasing temperatures, become ductile and n-type conductive (primarily conduct electrons). By contrast, the upper portion of the crust is assumed to be p-type conductive (primarily conduct p-holes). Under ideal modeling conditions as depicted in **Figure 6b** two outflow currents would develop, an electron current flowing downward into the lower crust and a p-hole current flowing horizontally in the thrust direction along the stress gradient. How the two currents reconnect is still very much an open question. Maybe electrolytical conductivity through the water-saturated gouge of deep faults provides a current path to close the circuit (Freund et al., 2004).

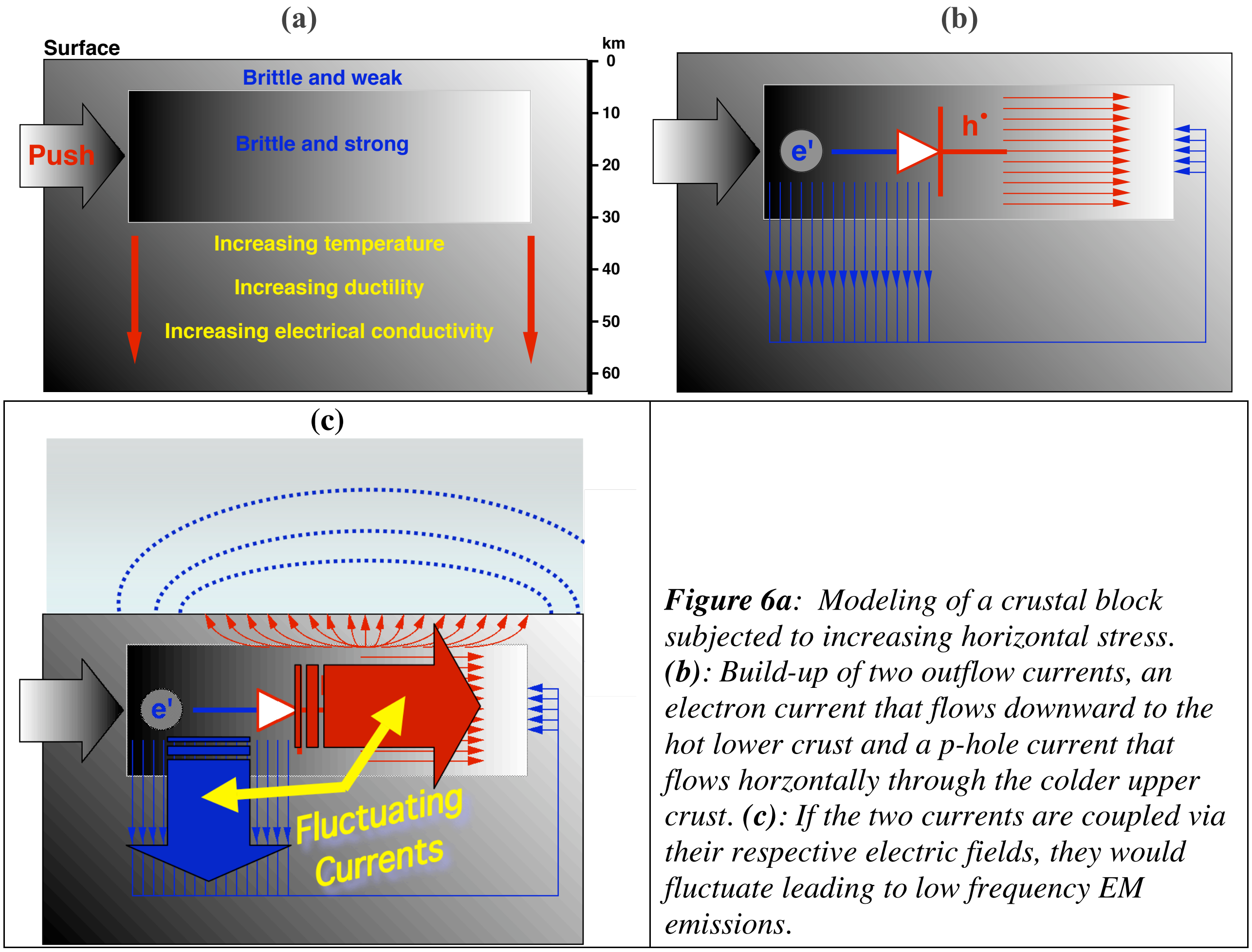

***Figure 6a**: Modeling of a crustal block subjected to increasing horizontal stress. (**b**): Build-up of two outflow currents, an electron current that flows downward to the hot lower crust and a p-hole current that flows horizontally through the colder upper crust. (**c**): If the two currents are coupled via their respective electric fields, they would fluctuate leading to low frequency EM emissions.*

The same mechanism, currents flowing through gouge-filled faults, may short-circuit a large portion of the stress-activated currents. However, if the volume of stressed rocks is on the order of 10^5 km^3 such as expected for tectonic situations that produce M=6.5 to M=7.5 earthquakes, and if each km^3 generate 10^5 A, the total amount of currents that can flow over an extended period of time, would indeed be very large. Even if 99.9% or more of the currents are “lost”, we might still have to consider transient telluric current systems in the 10^6 A range.

Figure 6c introduces the model concept that the electron and p-hole currents would be coupled via their respective electric fields and therefore be subject to fluctuations. Such fluctuations must then lead to electromagnetic (EM) emissions in the low frequency range. The parameters of the transient current systems will determine the spectral characteristics of the low frequency EM emissions. The magnitude of the currents will determine the emitted power per frequency band.

Conclusions

The model that we present here is based on laboratory data, which show that rocks under stress become a source of two outflow currents of equal magnitude but opposite sign. The model represents our first attempt to apply the insight gained from these laboratory experiments to geophysical situations, which are highly idealized but probably sufficiently close to reality to contain some kernel of truth.

A characteristic feature of our concept of fluctuating telluric currents is that it allows us to rationalize, in principle, why powerful low frequency EM emissions would become observable under certain conditions but remain unobservable in other cases. Their inobservability would be due to as yet poorly understood and poorly constrained processes in the Earth’s crust that can either prevent the postulated electron and p-hole currents altogether or redirect them in ways as to cancel their EM emissions.

Given the newly discovered dual outflow currents from stressed igneous rocks and their magnitudes as inferred from our laboratory data, our model allows us to consider powerful transient telluric currents – far more powerful than could be accounted for by any of the source mechanisms discussed in the literature based on piezoelectricity, fracto-electrification, and streaming potentials.

Acknowledgments

We thank Akthem Al-Manaseer, Dept. Civil and Environmental Engineering, San Jose State University, and Charles Schwartz, Dept. of Civil and Environmental Engineering, University of Maryland, College Park, MD, for providing access to hydraulic presses used in this study. This work was supported under grants from NASA Ames Research Center Director’s Discretionary Fund and NASA Goddard Space Flight Center GEST (Goddard Earth Science and Technology) program. Additional support was provided by NIMA (National Imaging and Mapping Agency) and by a scholarship to A. T. from JSPS (Japan Society for the Promotion of Science).

References

Biagi, P.F. et al., 2001. Hydrogeochemical precursors of strong earthquakes in Kamchatka: further analysis. Natural Hazards and Earth System Sciences, 1: 9-14.

Bianchi, R. and al., e., 1984. Radiofrequency emissions observed during macroscopic hypervelocity impact experiments. Nature, 308: 830-832.

Brace, W.F., 1975. Dilatancy-related electrical resistivity change in rocks. Pure Appl. Geophys., 113: 207-217.

Brace, W.F., Paulding, B.W. and Scholz, C., 1966. Dilatancy in the fracture of crystalline rocks. J. Geophys. Res., 71: 3939-3953.

Chadha, R.K., Pandey, A.P. and Kuempel, H.J., 2003. Search for earthquake precursors in well water levels in a localized seismically active area of Reservoir Triggered Earthquakes in India. Geophy. Res. Lett., 30: 69-71.

Derr, J.S., 1973. Earthquake lights: a review of observations and present theories. Bull. Seismol. Soc. Amer., 63: 2177-21287.

Enomoto, Y. and Hashimoto, H., 1990. Emission of charged particles form indentation fracture of rocks. Nature, 346: 641-643.

Freund, F., 2002. Charge generation and propagation in rocks. J. Geodynamics, 33: 545-572.

Freund, F. et al., 1994. Positive hole–type charge carriers in oxide materials. In: L.M. Levinson (Editor), Grain Boundaries and Interfacial Phenomena in Electronic Ceramics. Amer. Ceram. Soc., Cincinnati, OH, pp. 263-278.

Freund, F.T., 2003. On the electrical conductivity structure of the stable continental crust. J. Geodynamics, 35: 353-388.

Freund, F.T., Takeuchi, A., Lau, B.W.S. and Hall, C.G., 2004. Positive holes and their role during the build-up of stress prior to the Chi-Chi earthquake. In: K.-F. Ma (Editor), International Conference in Commemoration of 5th Anniversary of the 1999 Chi-Chi Earthquake, Taipei, Taiwan.

Fujinawa, Y., Matsumoto, T., Iitaka, H. and Takahashi, S., 2001. Characteristics of the Earthquake Related ELF/VLF Band Electromagnetic Field Changes, American Geophysical Union, Fall Meeting 2001. AGU, San Franscisco, CA, pp. #S42A-0616.

Fujinawa, Y. and Takahashi, K., 1990. Emission of electromagnetic radiation preceding the Ito seismic swarm of 1989. Nature, 347: 376 - 378.

Gershenzon, N. and Bambakidis, G., 2001. Modeling of seismo-electromagnetic phenomena. Russian J. Earth Scie., 3: 247-275.

Gerstenberger, M.C., Wiemer2, S., Jones, Lucile M. and Reasenberg, P.A., 2005. Real-time forecasts of tomorrow's earthquakes in California. Nature, 435: 328-331.

Goebel, E.D., Coveney, R.M., Angino, E.E., Zeller, E.J. and Dreschhoff, K., 1984. Geology, composition, isotopes of naturally occurring H_2/N_2 rich gas from wells near Junction City, Kansas. Oil & Gas, 82: 215-222.

Gokhberg, M.B., Morgounov, V.A., Yoshino, T. and Tomizawa, I., 1982. Experimental measurements of electromagnetic emissions possible related to earthquakes in Japan. J. Geophys. Res., 87: 7824-7828.

Hauksson, E., 1981. Radon content of groundwater as an earthquake precursor: Evaluation of worldwide data and physical basis. J. Geophys, Res., 86: 9397-9410.

Hayakawa, M., 1989. Satellite observation of low latitude VLF radio noise and their association with thunderstorms. J. Geomagn. Geoelectr., 41: 573-595.

Hazzard, J.F., Young, R.P. and Maxwell, S.C., 2000. Micromechanical modeling of cracking and failure in brittle rocks. J. Geophys. Res., 105: 16,683-16,697.

Igarashi, G., Tohjima, Y. and Wakita, H., 1993. Time-variable response characteristics of groundwater radon to earthquakes. Geophy. Res. Lett., 20: 1807-1810.

Igarashi, G. and Wakita, H., 1991. Tidal responses and earthquake-related changes in the water level of deep wells. J. Geophys, Res., 96: 4269-42-78.

Ivanov, B.A., Okulewskij, B.A. and Basilwvskij, A.T., 1976. Impulse magnetic field due to shock induced polarization in rocks as a possible cause of magnetic field anomalies on the moon, related to craters. Pisma v Asronomichelskij J., 2: 257-260.

King, B.V. and Freund, F., 1984. Surface charges and subsurface space charge distribution in magnesium oxide containing dissolved traces of water. Phys. Rev., B 29: 5814-5824.

King, C.-Y., 1983. Electromagnetic emission before earthquakes. Nature, 301: 377.

Kopytenko, Y.A., Matiashvili, T.G., Voronov, P.M., Kopytenko, E.A. and Molchanov, O.A., 1993. Detection of ultralow frequency emissions connected with the Spitak earthquake and its aftershock activity, based on geomagnetic pulsation data at Susheti and Vardzia observatories. Phys. Earth Planet. Inter., 77: 85-95.

Ma, Q.-z., Jing-yuan, Y. and Gu, X.-z., 2003. The electromagnetic anomalies observed at Chongming station and the Taiwan strong earthquake (M=7.5, March 31, 2002). Earthquake, 23: 49-56.

Marfunin, A.S., 1979. Spectroscopy, Luminescence and Radiation Centers in Minerals. Springer Verlag, New York, 257-262 pp.

Martelli, G. and Smith, P.N., 1989. Light, radiofrequency emission and ionization effects associated with rock fracture. Geophys, J. Internatl., 98: 397-401.

Martens, R., Gentsch, H. and Freund, F., 1976. Hydrogen release during the thermal decomposition of magnesium hydroxide to magensium oxide. J. Catalysis, 44: 366-372.

Molchanov, O.A. and Hayakawa, M., 1998. On the generation mechanism of ULF seimogenic electromagnetic emissions. Phys. Earth Planet. Int., 105: 201-220.

Nitsan, U., 1977. Electromagnetic emission accompanying fracture of quartz-bearing rocks. Geophys. Res. Lett., 4: 333-336.

Plastino, W., Bella, F., Catalano, P.G. and Di Giovambattista, R., 2002. Radon groundwater anomalies related to the Umbria-Marche, September 26, 1997, earthquakes. Geofisica Internacional, 41: 369-375.

Pulinets, S.A., Legen'ka, A.D. and Alekseev, V.A., 1994. Pre-earthquakes effects and their possible mechanisms, Dusty and Dirty Plasmas, Noise and Chaos in Space and in the Laboratory. Plenum Publishing, New York, pp. 545-557.

Rao, G., Reddy, G., Rao, R. and Gopalan, K., 1994. Extraordinary helium anomaly over surface rupture of September 1993 Killari earthquake, India. Current Science, 66: 933-936.

Sano, Y., Takahata, N., Igarashi, G., Koizumi, N. and others, a., 1998. Helium degassing related to the Kobe earthquake. Chemical Geology, 150: 171-179.

St-Laurent, F., 2000. The Saguenay, Québec, earthquake lights of November 1988-January 1989. Seismolog. Res. Lett., 71: 160-174.

Symons, M.C.R., 2001. Hole centers in MgO. Radiation Physics and Chemistry, 60: 39-41.

Takeuchi, A., Lau, B.W.S. and Freund, F.T., 2005. Current and surface potential induced by stress-activated positive holes in igneous rocks. Phys. Chem. Earth, this issue.

Takeuchi, A. and Nagahama, H., 2001. Voltage changes induced by stick-slip of granites. Geophys. Res. Lett., 28: 3365-3368.

Takeuchi, A. and Nagahama, H., 2002. Surface charging mechanism and scaling law related to earthquakes. J. Atmospheric Electricity, 22: 183-190.

Tsukuda, T., 1997. Sizes and some features of luminous sources associated with the 1995 Hyogo-ken Nanbu earthquake. J. Phys. Earth, 45: 73-82.

Vershinin, E.F., Buzevich, A.V., Yumoto, K., Saita, K. and Tanaka, Y., 1999. Correlation of seismic activity with electromagnetic emissions and variations in Kamchatka region. In: M. Hayakawa (Editor), Atmospheric and Ionospheric Electromagnetic Phenomena Associated with Earthquakes. Terra Sci. Publ., Tokyo, Japan, pp. 513-517.

Yasui, Y., 1973. A summary of studies on luminous phenomena accompanied with earthquakes. Memoirs Kakioka Magnetic Observatory, 15: 127-138.

Yen, H.-Y. et al., 2004. Geomagnetic fluctuations during the 1999 Chi-Chi earthquake in Taiwan. Earth Planets Space, 56: 39-45.

Yoshida, S., Manjgaladze, P., Zilpimiani, D., Ohnaka, M. and Nakatani, M., 1994. Electromagnetic emissions associated with frictional sliding of rock. In: M. Hayakawa and Y. Fujinawa (Editors), Electromagnetic Phenomena Related to Earthquake Prediction. Terra Scientific, Tokyo, pp. 307-322.

Yoshino, T. and Tomizawa, I., 1989. Observation of low-frequency electromagnetic emissions as precursors to the volcanic eruption at Mt. Mihara during November, 1986. Phys. Earth and Planet. Interiors, 57: 32 - 39.

Zlotnicki, J. and Cornet, F.H., 1986. A numerical model of earthquake-induced piezomagnetic anomalies. J. Geophys. Res., B91: 709-718.